Ultrasonics 94 (2019) 227–234

Contents lists available at ScienceDirect

Ultrasonics

journal homepage: www.elsevier.com/locate/ultras

Thermally tunable topological edge states for in-plane bulk waves in solid phononic crystals

Heng Liu, Shao-yong Huo, Lu-yang Feng, Hong-bo Huang, Jiu-jiu Chen*

State Key Laboratory of Advanced Design and Manufacturing for Vehicle Body, College of Mechanical and Vehicle Engineering, Hunan University, Changsha City 410082, People's Republic of China

ARTICLE INFO

Keywords:
Tunable edge states
In-plane bulk waves
Topological phononic crystals

ABSTRACT

The remarkable properties of topological insulators have inspired numerous studies on topological transport for bulk waves, but the demonstrations of topological edge states with tunable frequency are few attempts. Here, we report on the active frequency tunability of topologically protected edge states for in-plane bulk waves by applying a thermal field. We find that the center frequency of topological band gap is shifted down and the band width is enlarged as the temperature increases. Meanwhile, the frequency range of topologically protected edge states is also shifted to low frequency region with the higher temperature. Furthermore, the robust propagation of in-plane bulk waves along a desired path is demonstrated within different frequency bands. The tunable frequency for both topological band gaps and topologically protected edge states achieves the active control of the transport for in-plane bulk waves, which may dramatically facilitate practical applications of novel phononic devices.

1. Introduction

Topology, a pure modern mathematical concept, has stimulated extremely hot research interest in the field of physics and engineering [1–13]. The topological insulators is widely observed and realized in the electronic materials. One of the most unique properties of electronic topological insulators is the emergence of topologically protected one-way transport [14]. The electrons propagate along an interface between domains that have different topological characteristics. Though topological insulators are first observed in electronic systems, the observation has inspired a series of theoretical predications and experimental investigations in other analogous systems. For example, the concept of topological physics has been introduced to the field of photonics due to the significant similarities of band structure between electronic crystals and photonic crystals, which opens a new direction towards the study of topological states. Up to now, numerous investigations of topological transport for photons have been demonstrated from microwave to optical frequencies [15]. Some intriguing advancements of topological photonic states are obtained, such as immunity to backscattering, unparalleled tolerance towards defects/imperfections, and topological transport on the lattice edges.

Due to these remarkable hallmarks, topological properties are not only studied in photonic crystals but also introduced to the field of phononics [16–37]. In acoustic systems, Ni et al. [16] theoretically observed the topologically protected acoustic edge states transport by breaking time-reversal symmetry. Yves et al. [22] studied the possibility to induce topologically non-trivial acoustic states at the deep subwavelength scale. Zhang et al. [25] further experimentally realized acoustic valley pseudospin and topologically protected edge states. In elastic systems, Kim et al. [26] studied the experimental realization of topologically protected edge states of elastic waves with complete band gaps in 1D continuous structures and Yin et al. [27] demonstrated the existence of interface modes for both longitudinal and bending waves in elastic phononic crystals. Vila et al. [28] reported the observation of topological valley modes that the mirror symmetry is broken by arranging the localized masses at the nodes in a 2D hexagonal lattice. In addition, topological guiding of elastic waves [29] and topological valley-chiral edge states of Lamb waves [30] were also demonstrated in phononic crystal slabs. Our previous works theoretically studied the topologically protected transport of plate-mode waves [31] and bulk elastic waves [32]. However, an even greater challenge in topological phononic crystals is posed by the lack of the frequency tunability, which is essential for enhanced functionality in practical applications but relatively few attempts to study. It is desirable to introduce a certain degree of freedom to actively tune the frequency range of the band gaps and edge states in topological phononic crystals so as to satisfy functional needs. Due to the usually fixed geometry and constituents of topological insulators after the fabrication, some effective strategies to

* Corresponding author.
E-mail address: chen99nju@gmail.com (J.-j. Chen).

https://doi.org/10.1016/j.ultras.2018.09.006
Received 8 August 2018; Received in revised form 8 September 2018; Accepted 13 September 2018
Available online 14 September 2018
0041-624X/

deal with this challenge are necessarily taken into account. Here, we take inspiration from the band gap tunability of phononic crystals, in which the frequency range of band gaps varies with the intensity of applied field, such as electric field [38,39], magnetic field [40–42], or thermal field [43–47]. In a similar way, these physical fields can also be utilized for tuning the frequency range of topological band gaps and edge states. Due to the strongly temperature-dependent elastic properties of epoxy in our discussion, the effects of thermal field on the frequency tunability are taken into consideration here. The active frequency controllability for both topological band gaps and edge states has special advantage in fine-tunable information processing and medical imaging technology.

In this paper, the frequency tunability of both topological band gaps and topologically protected edge states for in-plane bulk waves is demonstrated in 2D solid-solid phononic crystals. As the temperature increases from 20 °C to 60 °C, the center position of topological band gap is shifted to lower frequency zone and the band width is enlarged with the higher temperature. Most importantly, the frequencies of topologically protected edge states are also shifted down with the increase of temperature. Finally, the robust propagation of in-plane bulk waves along a predefine path is further demonstrated within different bulk band gaps. The active frequency tunability of topologically protected edge states is realized in our discussion by changing the temperature, which may dramatically facilitate practical applications of topological elastic wave devices.

2. Theory and method

Fig. 1a shows the schematic diagram of the system we proposed. The system is that the epoxy cylinders embedded in a honeycombed ceramic netted matrix. The pristine honeycomb lattice of individual atomic sites is to be considered as a triangular lattice of hexagons with the characteristic of C_6-symmerty, marked by a red dash line in Fig. 1a. The structural parameters of the system are: the lattice constant $a = 4$ mm, the diameter of the large ceramic cylinders $D = 1.56$ mm, the diameter of the small epoxy cylinders $d = 1.20$ mm, and the width of the connecting band $b = 0.30$ mm, respectively. As a typical and widely used engineering material, epoxy possesses special mechanical properties that strongly depend on the temperature [48,49]. In our discussion, the temperature only influences the Young's modulus and shear modulus of epoxy and the mass density is assumed to be temperature-independent. The Young's modulus and shear modulus of epoxy are given in Table 1 and the mass density is 1180 kg/m^3 [50], respectively. The Young's modulus, Poisson's ratio and mass density for ceramic are $E = 110.4$ GPa, $\mu = 0.256$ and $\rho = 3050$ kg/m^3, respectively [51]. Base on the zone folding mechanism, the Brillouin zones (BZs) will be converted to the small 30°-rotated hexagon as shown in Fig. 1b and the K symmetry point is folded to the Γ symmetry point.

Table 1
The temperature-dependent Young's modulus (E) and shear modulus (G) of epoxy.

Temperature/°C	20	30	40	50	60
E/GPa	12.9	12	10.4	6.7	1
G/GPa	4.925	4.615	4	2.575	0.385

The elastic wave equation in an inhomogeneous, linear, isotropic medium with no body force has the following form [52]:

$$\rho(\vec{r})\ddot{u}_i(\vec{r},t) = \frac{\partial}{\partial x_i}\left[\lambda(\vec{r},T)\frac{\partial u_j(\vec{r},t)}{\partial x_j}\right] + \frac{\partial}{\partial x_j}\left[\mu(\vec{r},T)\left(\frac{\partial u_i(\vec{r},t)}{\partial x_j}+\frac{\partial u_j(\vec{r},t)}{\partial x_i}\right)\right], \quad (1)$$

where $u_i(\vec{r},t)$ is the displacement vector of the ith component, $\rho(\vec{r})$ is the position-dependent mass density, $\lambda(\vec{r},T)$ and $\mu(\vec{r},T)$ are the position-dependent and temperature-dependent Lame coefficients, respectively. As the temperature increases, the relationships between the Young's modulus E, shear modulus G and the Lame coefficients always follow the same equations [50]:

$$\lambda = \frac{G(E-2G)}{3G-E}, \quad (2)$$

$$\mu = G \quad (3)$$

In isotropic medium, the 2D bulk elastic wave field is decoupled. So, the wave Eq. (1) can split into two decoupled independent equations, one for out-of-plane modes (u_z) and the other for mixed in-plane modes (u_x and u_y), respectively. The mixed in-plane modes studied here include both longitudinal and transverse waves. The corresponding equations are the following form:

$$\rho\omega^2 u_x + \frac{\partial}{\partial x}\left[(\lambda+2\mu)\frac{\partial u_x}{\partial x}+\lambda\frac{\partial u_y}{\partial y}\right] + \frac{\partial}{\partial y}\left[\mu\left(\frac{\partial u_x}{\partial y}+\frac{\partial u_y}{\partial x}\right)\right] = 0, \quad (4)$$

$$\rho\omega^2 u_y + \frac{\partial}{\partial x}\left[\mu\left(\frac{\partial u_x}{\partial y}+\frac{\partial u_y}{\partial x}\right)\right] + \frac{\partial}{\partial y}\left[\lambda\frac{\partial u_x}{\partial x}+(\lambda+2\mu)\frac{\partial u_y}{\partial y}\right] = 0 \quad (5)$$

According to the Bloch-Floquet theorem, the mass density (ρ), the Lame coefficients (λ and μ) and the displacement (u_i) can be expanded in Fourier series at the corresponding temperature T as [52]

$$\Phi(\boldsymbol{r},T) = \sum_{\boldsymbol{G}} e^{i\boldsymbol{G}\cdot\boldsymbol{r}}\Phi_{\boldsymbol{G}}(T), \quad (6)$$

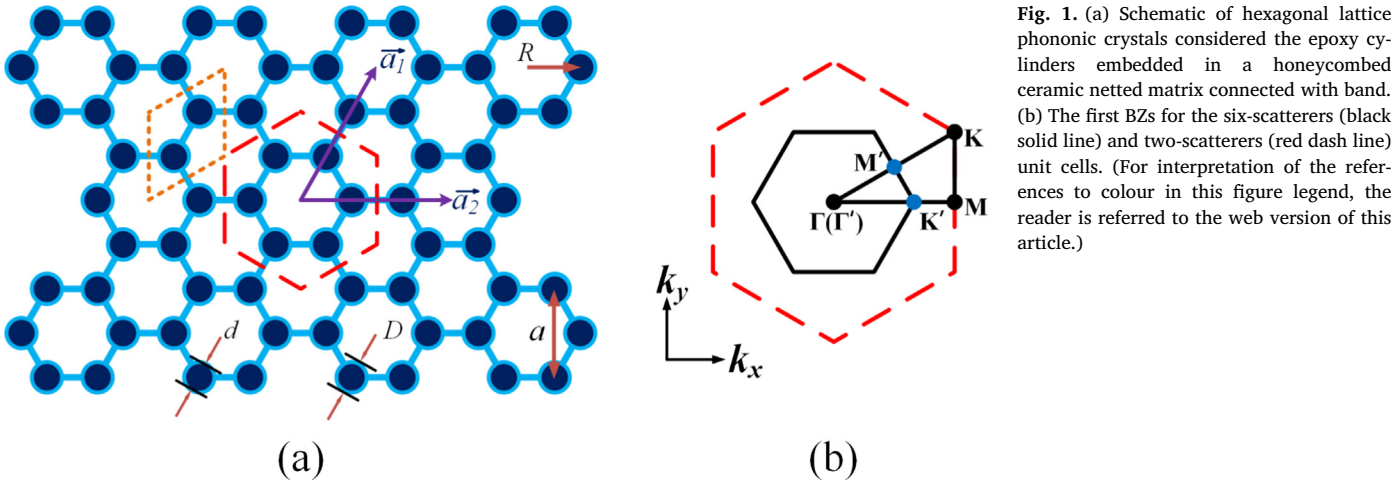

Fig. 1. (a) Schematic of hexagonal lattice phononic crystals considered the epoxy cylinders embedded in a honeycombed ceramic netted matrix connected with band. (b) The first BZs for the six-scatterers (black solid line) and two-scatterers (red dash line) unit cells. (For interpretation of the references to colour in this figure legend, the reader is referred to the web version of this article.)

$$u(\boldsymbol{r}, \boldsymbol{k}) = \sum_{G'} e^{i\boldsymbol{k}\cdot\boldsymbol{r}-i\omega t}(e^{i\boldsymbol{G}'\cdot\boldsymbol{r}}u_k(\boldsymbol{G}')), \tag{7}$$

where $\boldsymbol{k}$ is the wave vector, $\boldsymbol{G}$ and $\boldsymbol{G}'$ are the vectors of the reciprocal lattice, Φ represents the mass density (ρ) and the Lame coefficients (λ and μ), and $\Phi_G(T)$ means the Fourier coefficients at the corresponding temperature T. Substituting Eqs. (6) and (7) into Eqs. (4) and (5), we can obtain the generalized eigenvalue equation of finite element method [53]:

$$[K(\boldsymbol{k}) - \omega^2 M]\boldsymbol{u} = 0, \tag{8}$$

where $\boldsymbol{K}$ and $\boldsymbol{M}$ are the stiffness and mass matrices, respectively. The band structure can be obtained by solving the eigenvalue problem within the primitive unit. A simplified approach is that the wave vectors $\boldsymbol{k}$ is utilized for sweeping along the boundary of the irreducible BZ (M → Γ → K → M).

The key physics that realizes a phononic topological insulator is to increase the degree of freedom to further create a double Dirac cone [54]. Therefore, it is necessary to adopt a deliberate strategy to form a fourfold degeneracy of band structure. A single Dirac cone first obtained within the primitive unit (marked by an orange dash line in Fig. 1a) and a double Dirac cone is further formed on the center of BZ based on a simple folding transformation mechanism [55]. A method proposed by Wu et al. [56] in the context of photonic crystals is adopted to tailor the topological properties of the crystalline metamaterial, which considers C_6-symmerty triangular lattices of expanded or shrunken hexagons. The method is based on the fact that the C_6-symmerty point group has two 2D irreducible representations, which correspond to even and odd parities respective to spatial inversion operation. We turn to the realization of frequency tunability for both topological band gaps and edge states after obtaining topological band gaps and edge states. The elastic properties of some smart material are thermal-sensitive. Hence, the application of a thermal field is taken into consideration here due to the strongly temperature-dependent elastic properties of epoxy in our discussion. The frequency ranges for both topological band gaps and topologically protected edge states can be tuned by changing the intensity of the applied thermal field.

3. Results and discussion

As shown in Fig. 2a, b, we first calculate the band structures before zone folding and after zone folding at T = 20 °C, respectively. It is shown in Fig. 2b that a double Dirac cone is achieved at Γ' point. Having obtained a double Dirac cone, we can focus on opening a topological band gap and tailoring the topological properties of our system. Here, we expand or shrink the six epoxy cylinders in the large unit cell to break the lattice symmetry and the schematic of which is shown in Fig. 3. The corresponding band structures for expanded clusters ($R = 0.60a$) and shrunken clusters ($R = 0.56a$) are calculated as shown in Fig. 3a, b, respectively. Obviously, two twofold degeneracy, one for the lower bands and the other for the upper bands, appear at the BZ center because the symmetry of the lattice is broken. At the same time, a topological band gap is opened around the Dirac point. According to quantum mechanics, the two twofold degeneracy always be classified as a pair of dipolar modes (p_x/p_y) and a pair of quadrupolar modes ($d_{xy}/d_{x^2-y^2}$). The dipoles are even or odd symmetrical to the axes x/y (corresponding to p_x/p_y), while the quadrupole is odd symmetrical to the axes x and y (corresponding to d_{xy}), or even symmetrical to the axes x and y at the same time (corresponding to $d_{x^2-y^2}$). The corresponding eigenfield distributions for both expanded clusters ($R = 0.60a$) and shrunken clusters ($R = 0.56a$) are calculated as shown in Fig. 3c, respectively. For expanded clusters, the lower twofold degeneracy states have a pair of dipolar states and the upper twofold degeneracy states have a pair of quadrupolar states, which opens a topologically trivial band gap. By comparing the eigenstates at the Γ' point between expanded clusters and shrunken clusters, we find that a reversal of eigenstates is obtained between dipolar modes and quadrupolar modes. That is to say, for shrunken clusters, the dipole modes rise above the quadrupole states. This reversal leads to an inverted band structure and gives rise to a nontrivial band topology. Meanwhile, the reversal of the band structure indicates that the band topology changes with the ratio of R/a.

The elastic properties of epoxy are strongly temperature-dependent. As shown in Table 1, the increasing temperature leads to significant changes both in the Young's modulus and shear modulus. The Young's modulus decreases from 12.9 GPa to 1 GPa and the shear modulus decreases from 4.925 GPa to 0.385 GPa. The band structure of corresponding phononic crystals may be proportionally scaled by changing the temperature. To demonstrate it, we calculate the band structures for both expanded and shrunken structure at different temperatures as shown in Fig. 4. For shrunken structure, the center frequency of the topologically nontrivial band gap is 817.56 kHz at 20 °C and 759.75 kHz at 40 °C, respectively. The corresponding band width is 33.27 kHz at 20 °C and 37.75 kHz at 40 °C, respectively. When temperature increases to 60 °C, a significant change emerge where the center frequency is shifted to 484.46 kHz and the band width is enlarged to 74.84 kHz. The topological band gap is shifted to low frequency zone with higher temperature. Fig. 5 shows the center frequency and band width of the topological band gaps for expanded and shrunken clusters when temperature increases from 20 °C to 60 °C. It is

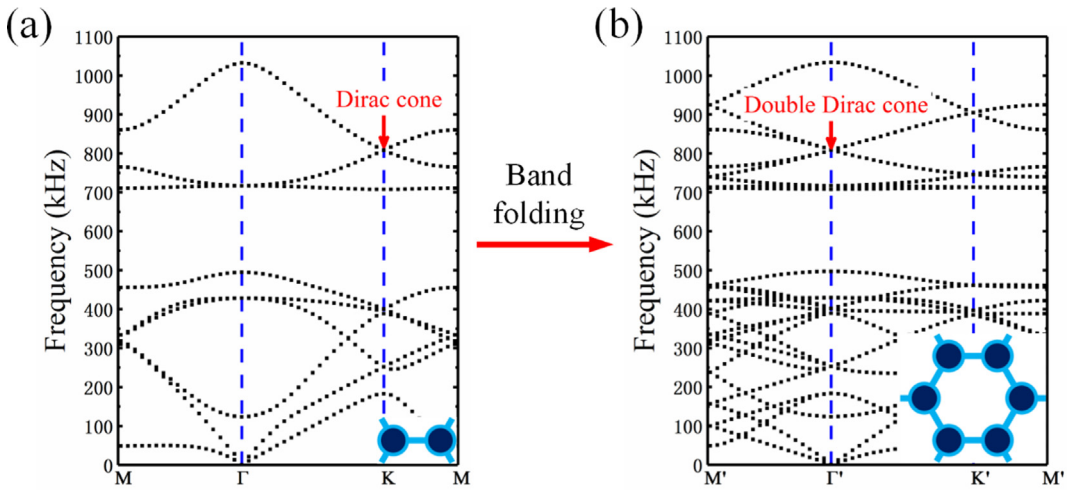

Fig. 2. (a) Band structure of undeformed structure based on the primitive unit cell containing two neighboring scatterers and a Dirac cone is formed at point K. (b) A double Dirac cone formed at the Γ' point by band folding. Inset: The schematic diagram of the primitive unit cell.

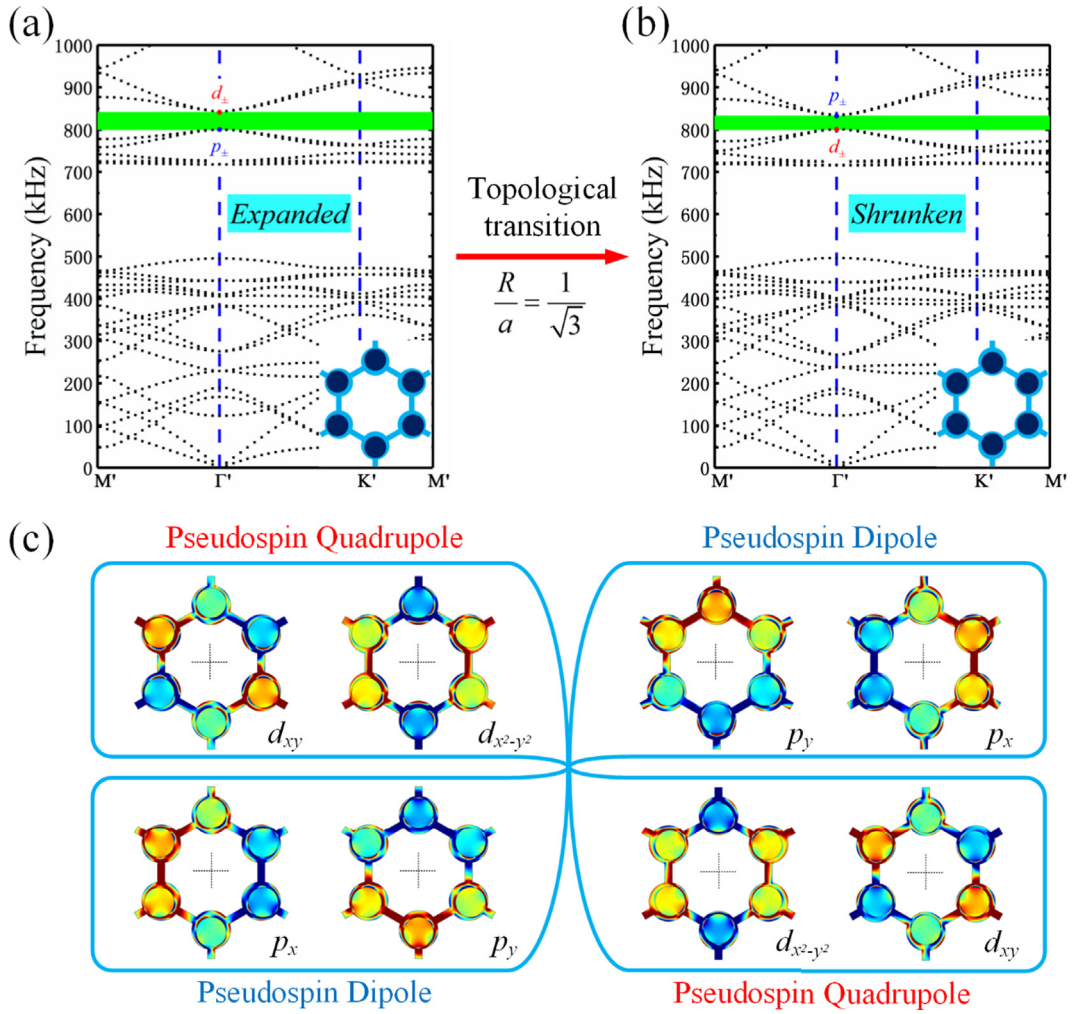

Fig. 3. (a) and (b) Band structures of symmetry broken unit cells with expanded clusters ($R = 0.60a$) and shrunken clusters ($R = 0.56a$) when T = 20 °C. Inset: The schematic diagram of expanded and shrunken six-scatterers for the large unit cell. (c) The field distributions of the pseudospin dipolars and quadrupolars for expanded clusters ($R = 0.60a$) and shrunken clusters ($R = 0.56a$).

obvious that the center frequency of the topologically nontrivial band gap for shrunken clusters is shifted down and the band width is enlarged with the increase of temperature. The topologically trivial band gap for expanded clusters has the same changes with the higher temperature. It means that the position and band width of the topological band gaps for both shrunken clusters and expanded clusters can be dynamically tuned by varying the temperature.

One of the key manifestations of topological insulators is the pesudospin-dependent unidirectional edge states. The special edge states emerge from the boundary between domains that have different band topologies. To obtain the edge states and study its frequency tunability, we consider a ribbon-shaped supercell. The supercell is composed of the topologically trivial crystals ($R = 0.60a$, 10 unit cells) located at the left and topologically nontrivial crystals ($R = 0.56a$, 10 unit cells) located at the right. The absorbing boundary condition is imposed along the left and right edges of the supercell. Meanwhile, the periodic boundary condition is introduced in the other direction of the lattice vector. Fig. 6a shows the band structure of the supercell with T = 20 °C. Two additional states appear in the frequency range of bulk gap between 802.78 kHz and 837.63 kHz as indicated by the red solid curves. Fig. 6d, e show the distributions of the real-space displacement field on the interface for the eigenstates at the solid curves around the Γ' point (labeled by black point A and blue point B in Fig. 6a with $k_x = \pm 0.1(\pi/a)$), respectively. The displacement field is confined at the interface and decays exponentially into bulk crystals on both sides. It means that the solid curves represent the dispersion relations of edge states that are tightly confined around the interface between the topologically nontrivial and trivial phases. At the same time, we plot the local magnified view where black arrows indicate the time-averaged Poynting vectors. The Poynting vectors exhibit a nonzero anticlockwise (clockwise) time-averaged mechanical energy flux ($I_j = -\sigma_{ij}v_j$, where σ_{ij} and v_j are stress tensor and velocity vector, respectively) for the pseudospin-up (pseudospin-down) state even averaged over time. Note that, the structures at the interface between the trivial and nontrivial domains do not have the same deformation. The C_6 crystalline symmetry of the boundary is effectively broken. So, a tiny gap will opens in the edge states around the Γ' point. Even so, the corresponding topological properties remain valid. Fig. 6b, c show the band structures of the edge modes at the same ribbon-shaped supercell for T = 40 °C and T = 60 °C, respectively. It is obvious that the frequencies of topologically edge states are shifted to lower frequency zone with the increase of temperature, which provides a new approach to dynamically tune the frequencies of the edge states without changing the structure or constitutes of system. The dynamic controllability for topological edge states makes it flexible for the practical application of topological phononic insulators.

A main exotic property of topological edge states that distinguishes them from their topologically trivial counterparts is robustness. We consider an interface between two distinct domains to demonstrate the robustness of topological edge states. An excitation source is placed on

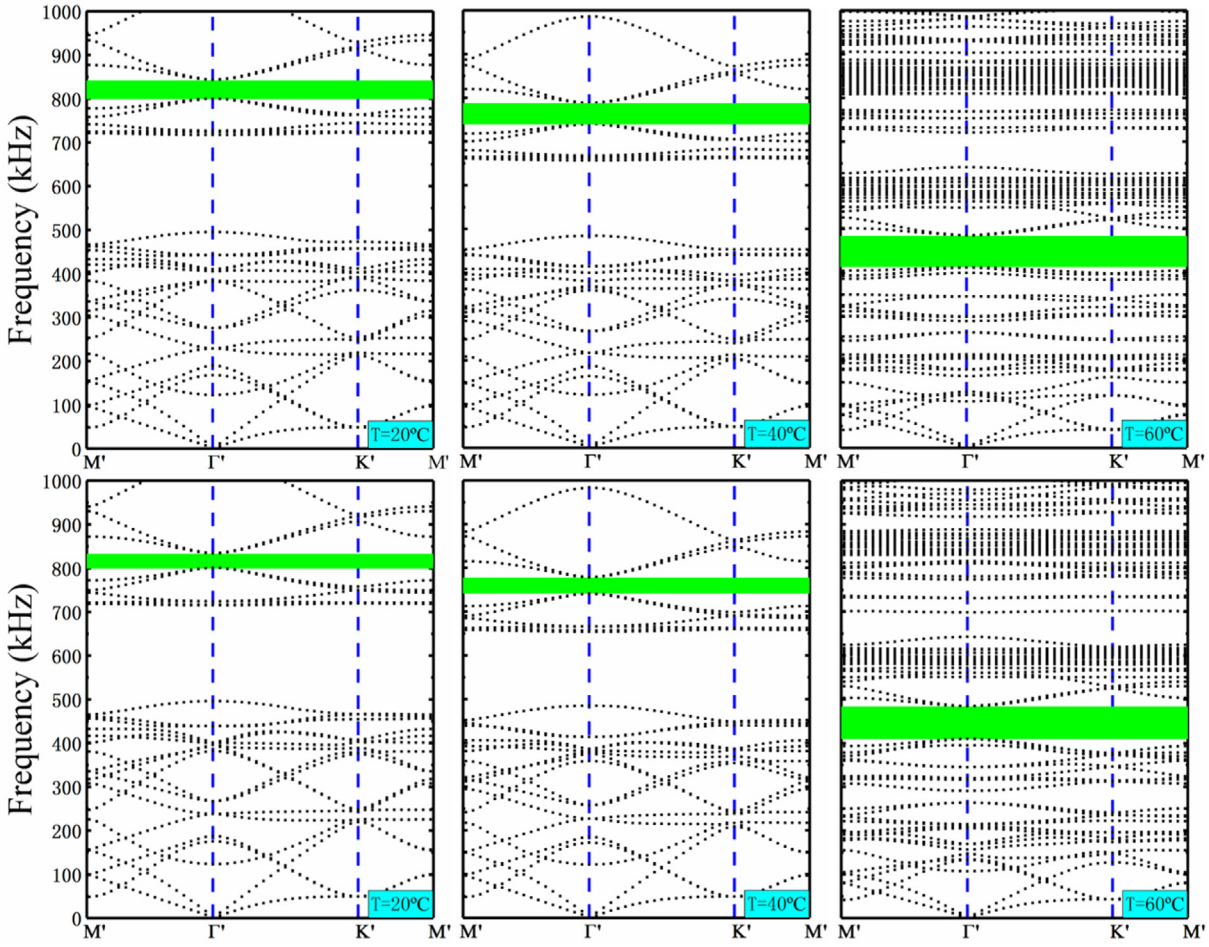

Fig. 4. Band structures with expanded clusters (top) and shrunken clusters (bottom) when T = 20 °C, 40 °C and 60 °C, respectively.

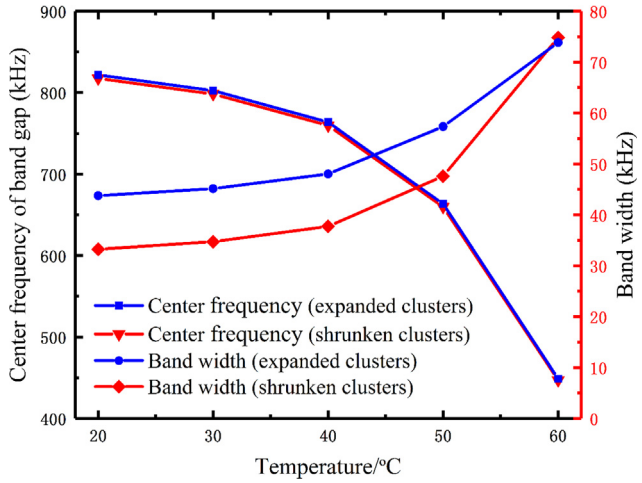

Fig. 5. Center frequency and band width of the topological band gaps for both expanded clusters ($R = 0.60a$, blue dash-dotted line) and shrunken clusters ($R = 0.56a$, red dash-dotted line) when the temperature changes from 20 °C to 60 °C. (For interpretation of the references to colour in this figure legend, the reader is referred to the web version of this article.)

the left side of the interface as shown in Fig. 7a. Fig. 7b–d show the displacement distributions of the edge states with the following temperature and frequency: 814 kHz at 20 °C, 759 kHz at 40 °C, and 446 kHz at 60 °C, respectively. Remarkably, there is no obvious backscattering in the edge states due to the topological protection. Moreover, the in-plane bulk waves can robust against local lattice defects/imperfections and disorder in the interface. In order to further confirm the topological robustness of the edge states, we deliberately introduce different kinds of defects into the interface and investigate their influence as shown in Fig. 8. It can be seen that the propagation of the in-plane bulk waves is immune to backscattering by self-detouring around the disordered region or reorganizing the field distributions in the local defects. These results suggest that topological protection is not affected by local defects. It provides a robust and dynamically frequency-tunable transport for in-plane bulk waves along arbitrary paths.

4. Conclusion

In conclusion, the active frequency tunability of the topological band gaps and topologically protected edge states for in-plane bulk waves is demonstrated through numerical simulation. The strongly temperature-dependent elastic properties of epoxy are taken into consideration in our discussion. When the temperature increases from 20 °C to 60 °C, for both shrunken clusters and expanded clusters, the center position of topological band gap is shifted down and the band width is enlarged. Most importantly, the frequencies of topological edge states are also shifted to low frequency zone with the increase of temperature. The active control of the frequency range for topologically protected edge states is realized by changing the temperature. In addition, the robust propagation of in-plane bulk elastic waves along a desired path is further demonstrated at different temperatures. These prominent features of the frequency tunability for both topological band gaps and topologically protected edge states provide a new route to implement unique tunable functionalities, which has special advantage for the

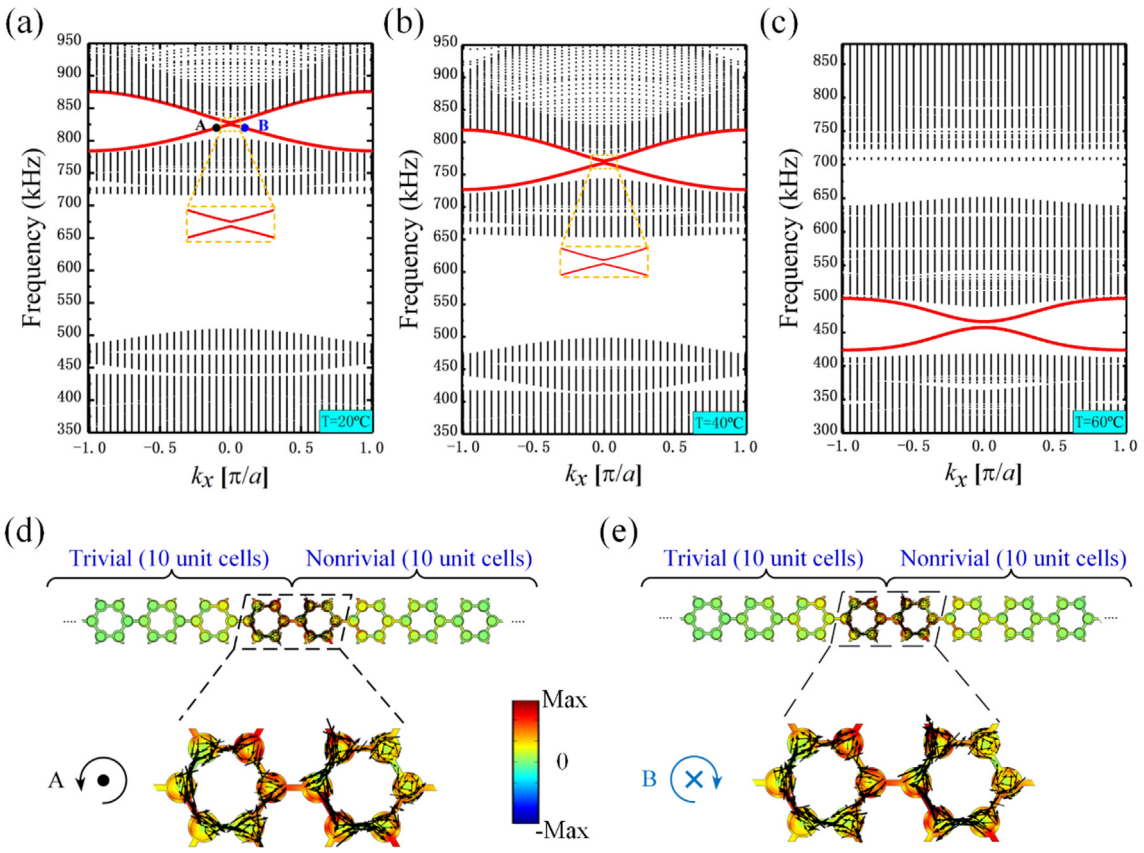

Fig. 6. (a)–(c) Band structures of supercell with topological edges modes shown by the red solid curves when T = 20 ˚C, 40 ˚C and 60 ˚C, respectively. Inset: The local magnified view of the tiny gap between two red solid curves. (d) and (e) Real-space displacement field distributions and the time-averaged Poynting vectors distributions at the interface with distinct topologies. (For interpretation of the references to colour in this figure legend, the reader is referred to the web version of this article.)

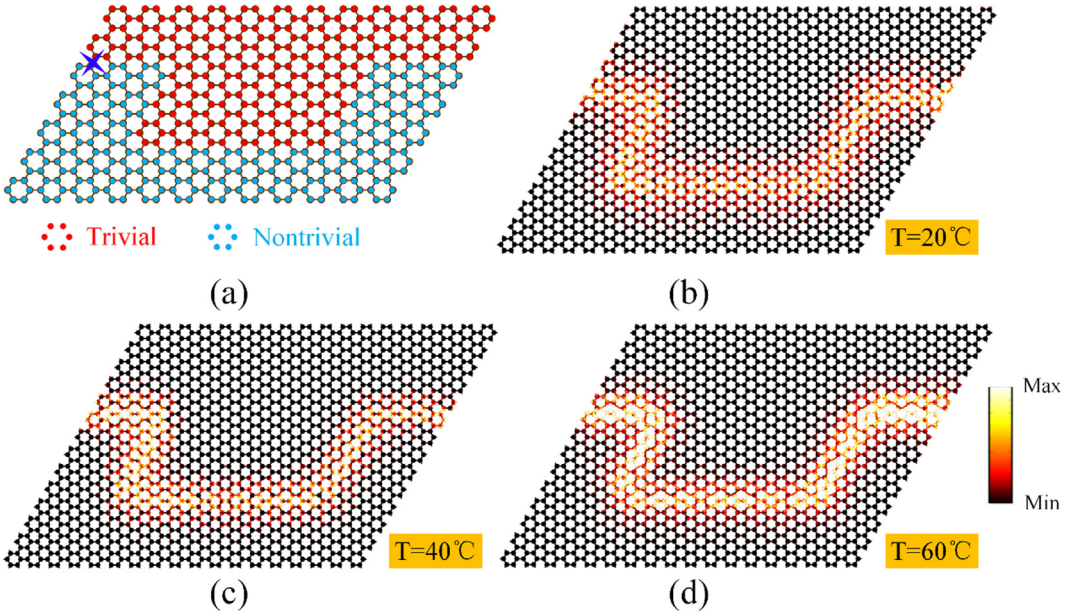

Fig. 7. (a) Schematic diagram of a desired boundary between trivial and nontrivial domains and an excitation source placed on the left side of the boundary. (b)–(d) the displacement field distributions of the in-plane bulk waves propagating in the channels with different frequencies and temperatures.

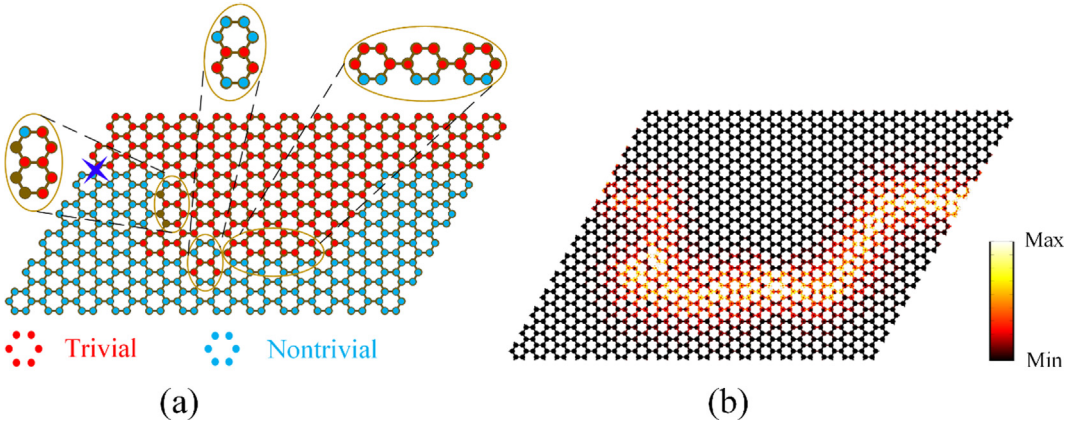

Fig. 8. (a) Schematic diagram of different kinds of defects (cavity and disorder) introduced to further verify the robustness of topologically protected one-way edge states. (b) Displacement distributions of in-plane bulk waves through the channels when T = 20 °C.

designing of integrated topological phononic devices.

Acknowledgements

The authors gratefully acknowledge financial support from National Science Foundation of China under Grant No. 11374093 and Young Scholar fund sponsored by common university and college of the province in Hunan.

Appendix A. Supplementary material

Supplementary data to this article can be found online at https://doi.org/10.1016/j.ultras.2018.09.006.

References

[1] B.A. Bernevig, T.L. Hughes, S.C. Zhang, Quantum spin Hall effect and topological phase transition in HgTe quantum wells, Science 314 (2006) 1757–1761.
[2] F.D.M. Haldane, S. Raghu, Possible realization of directional optical waveguides in photonic crystals with broken time-reversal symmetry, Phys. Rev. Lett. 100 (2008) 013904.
[3] M.Z. Hasan, C.L. Kane, Colloquium: topological insulators, Rev. Mod. Phys. 82 (2010) 3045–3067.
[4] X.L. Qi, S.C. Zhang, Topological insulators and superconductors, Rev. Mod. Phys. 83 (2011) 1057–1110.
[5] A.B. Khanikaev, S.H. Mousavi, W.K. Tse, M. Kargarian, A.H. MacDonald, G. Shvets, Photonic topological insulators, Nat. Mater. 12 (2013) 233–239.
[6] S. Rodriguez, M. Deschamps, M. Castaings, E. Ducasse, Guided wave topological imaging of isotropic plates, Ultrasonics 54 (2014) 1880–1890.
[7] C.X. Bai, K.W. Wei, Y.Y. Shen, Y.L. Yang, The effect of ferromagnetism on the critical supercurrent in topological insulator Josephson junction, Appl. Phys. A-Mater. 121 (2015) 1139–1146.
[8] R. Susstrunk, S.D. Huber, Observation of phononic helical edge states in a mechanical topological insulator, Science 349 (2015) 47–50.
[9] Y.G. Peng, Z.G. Geng, X.F. Zhu, Topologically protected bound states in one-dimensional Floquet acoustic waveguide systems, J. Appl. Phys. 123 (2018) 091716.
[10] J.J. He, Z. Kang, Achieving directional propagation of elastic waves via topology optimization, Ultrasonics 82 (2018) 1–10.
[11] Z.G. Geng, Y.G. Peng, Y.X. Shen, D.G. Zhao, X.F. Zhu, Topologically protected edge transport of sound in coupled cavities of a modified honeycomb lattice, J. Phys.: Condens. Matter 30 (2018) 345401.
[12] M. Serra-Garcia, V. Peri, R. Susstrunk, O.R. Bilal, T. Larsen, L.G. Villanueva, S.D. Huber, Observation of a phononic quadrupole topological insulator, Nature 555 (2018) 342–345.
[13] H.C. Tang, Z.S. Chen, N. Tang, S.F. Li, Y.X. Shen, Y.G. Peng, X.F. Zhu, J.F. Zang, Hollow-out patterning ultrathin acoustic metasurfaces for multifunctionalities using soft fiber/rigid bead networks, Adv. Funct. Mater. 1801127 (2018).
[14] F. Gao, Z. Gao, X.H. Shi, Z.J. Yang, X. Lin, H.Y. Xu, J.D. Joannopoulos, M. Soljacic, H.S. Chen, L. Lu, Y.D. Chong, B.L. Zhang, Probing topological protection using a designer surface plasmon structure, Nat. Commun. 7 (2016) 11619.
[15] X. Cheng, C. Jouvaud, X. Ni, S.H. Mousavi, A.Z. Genack, A.B. Khanikaev, Robust reconfigurable electromagnetic pathways within a photonic topological insulator, Nat. Mater. 15 (2016) 542–549.
[16] X. Ni, C. He, X.C. Sun, X.P. Liu, M.H. Lu, L. Feng, Y.F. Chen, Topologically protected one-way edge mode in networks of acoustic resonators with circulating air flow, New J. Phys. 17 (2015) 053016.
[17] M. Xiao, G.C. Ma, Z.Y. Yang, P. Sheng, Z.Q. Zhang, C.T. Chan, Geometric phase and band inversion in periodic acoustic systems, Nat. Phys. 11 (2015) 240–244.
[18] Z.J. Yang, F. Gao, X.H. Shi, X. Lin, Z. Gao, Y.D. Chong, B.L. Zhang, Topological acoustics, Phys. Rev. Lett. 114 (2015) 114301.
[19] P. Wang, L. Lu, K. Bertoldi, Topological phononic crystals with one-way elastic edge waves, Phys. Rev. Lett. 115 (2015) 104302.
[20] Y.G. Peng, C.Z. Qin, D.G. Zhao, Y.X. Shen, X.Y. Xu, M. Bao, H. Jia, X.F. Zhu, Experimental demonstration of anomalous Floquet topological insulator for sound, Nat. Commun. 7 (2016) 13368.
[21] J. Mei, Z.G. Chen, Y. Wu, Pseudo-time-reversal symmetry and topological edge states in two-dimensional acoustic crystals, Sci. Rep. 6 (2016) 32752.
[22] S. Yves, R. Fleury, F. Lemoult, M. Fink, G. Lerosey, Topological acoustic polaritons: robust sound manipulation at the subwavelength scale, New J. Phys. 19 (2017) 075003.
[23] S.Y. Huo, J.J. Chen, H.B. Huang, G.L. Huang, Simultaneous multi-band valley-protected topological edge states of shear vertical wave in two-dimensional phononic crystals with veins, Sci. Rep. 7 (2017) 10335.
[24] J. Li, J. Wang, S. Wu, J. Mei, Pseudospins and topological edge states in elastic shear waves, AIP Adv. 7 (2017) 125030.
[25] Z.W. Zhang, Y. Tian, Y. Cheng, Q. Wei, X.J. Liu, J. Christensen, Topological acoustic delay line, Phys. Rev. Appl. 9 (2018) 034032.
[26] I. Kim, S. Iwamoto, Y. Arakawa, Topologically protected elastic waves in one-dimensional phononic crystals of continuous media, Appl. Phys. Exp. 11 (2018) 017201.
[27] J.F. Yin, M. Ruzzene, J.H. Wen, D.L. Yu, L. Cai, L.F. Yue, Band transition and topological interface modes in 1D elastic phononic crystals, Sci. Rep. 8 (2018) 6806.
[28] J. Vila, R.K. Pal, M. Ruzzene, Observation of topological valley modes in an elastic hexagonal lattice, Phys. Rev. B 96 (2017) 134307.
[29] Y.N. Guo, T. Dekorsy, M. Hettich, Topological guiding of elastic waves in phononic metamaterials based on 2D pentamode structures, Sci. Rep. 7 (2017) 18043.
[30] J. Wang, J. Mei, Topological valley-chiral edge states of Lamb waves in elastic thin plates, Appl. Phys. Exp. 11 (2018) 057302.
[31] J.J. Chen, S.Y. Huo, Z.G. Geng, H.B. Huang, X.F. Zhu, Topological valley transport of plate-mode waves in a homogenous thin plate with periodic stubbed surface, AIP Adv. 7 (2017) 115215.
[32] S.Y. Huo, J.J. Chen, H.B. Huang, Topologically protected edge states for out-of-plane and in-plane bulk elastic waves, J. Phys.: Condens. Matter 30 (2018) 145403.
[33] Y.G. Peng, Y.X. Shen, D.G. Zhao, X.F. Zhu, Low-loss and broadband anomalous Floquet topological insulator for airborne sound, Appl. Phys. Lett. 110 (2017) 173505.
[34] R. Chaunsali, C.W. Chen, J.Y. Yang, Subwavelength and directional control of flexural waves in zone-folding induced topological plates, Phys. Rev. B 97 (2018) 054307.
[35] R.K. Pal, J. Vila, M. Leamy, M. Ruzzene, Amplitude-dependent topological edge states in nonlinear phononic lattices, Phys. Rev. E 97 (2018) 032209.
[36] Z.G. Geng, Y.G. Peng, Y.X. Shen, D.G. Zhao, X.F. Zhu, Acoustic delay-line filters based on largely distorted topological insulators, Appl. Phys. Lett. 113 (2018) 033503.
[37] S.Y. Yu, C. He, Z. Wang, F.K. Liu, X.C. Sun, Z. Li, H.Z. Lu, M.H. Lu, X.P. Liu, Y.F. Chen, Elastic pseudospin transport for integratable topological phononic circuits, Nat. Commun. 9 (2018) 3072.
[38] Y.Z. Wang, F.M. Li, W.H. Huang, X.A. Jiang, Y.S. Wang, K. Kishimoto, Wave band gaps in two-dimensional piezoelectric/piezomagnetic phononic crystals, Int. J. Solids. Struct. 45 (2008) 4203–4210.
[39] Y.Z. Wang, F.M. Li, K. Kishimoto, Y.S. Wang, W.H. Huang, Wave band gaps in three-dimensional periodic piezoelectric structures, Mech. Res. Commun. 36 (2009) 461–468.
[40] O.B. Matar, J.F. Robillard, J.O. Vasseur, A.C. Hladky-Hennion, P.A. Deymier, P. Pernod, V. Preobrazhensky, Band gap tunability of magneto-elastic phononic crystal, J. Appl. Phys. 111 (2012) 054901.
[41] S.Z. Zhang, Y. Shi, Y.W. Gao, A mechanical-magneto-thermal model for the

tunability of band gaps of epoxy/Terfenol-D phononic crystals, J. Appl. Phys. 118 (2015) 034101.
[42] C.J. Zhou, Y. Sai, J.J. Chen, Tunable Lamb wave band gaps in two-dimensional magnetoelastic phononic crystal slabs by an applied external magnetostatic field, Ultrasonics 71 (2016) 69–74.
[43] K.L. Jim, C.W. Leung, S.T. Lau, S.H. Choy, H.L.W. Chan, Thermal tuning of phononic bandstructure in ferroelectric ceramic/epoxy phononic crystal, Appl. Phys. Lett. 94 (2009) 193501.
[44] Y. Cheng, X.J. Liu, D.J. Wu, Temperature effects on the band gaps of Lamb waves in a one-dimensional phononic-crystal plate (L), J. Acous. Soc. Am. 129 (2011) 1157–1160.
[45] Y.W. Yao, F.G. Wu, X. Zhang, Z.L. Hou, Thermal tuning of Lamb wave band structure in a two-dimensional phononic crystal plate, J. Appl. Phys. 110 (2011) 123503.
[46] Z.G. Bian, W. Peng, J.Z. Song, Thermal tuning of band structures in a one-dimensional phononic crystal, J. Appl. Mech-T. Asme. 81 (2014) 041008.
[47] Z.J. Chen, Thermal tuning of omnidirectional reflection bands in one-dimensional finite phononic crystals, J. Appl. Phys. 117 (2015) 124902.
[48] E.L. Klamer, D.A. Hordijk, M.C.J. Hermes, The influence of temperature on RC beams strengthened with externally bonded CFRP reinforcement, Indian Concr. J. 53 (2008) 157–186.
[49] O. Rabinovitch, Impact of thermal loads on interfacial debonding in FRP strengthened beams, Int. J. Solids. Struct. 47 (2010) 3234–3244.
[50] X.L. Zhou, J.L. Chen, Y.H. Li, Y.X. Sun, Y.F. Xing, Thermal tuning on band gaps of 2D phononic crystals considering adhesive layers, J. Phys. D. Appl. Phys. 51 (2018) 075105.
[51] Y. Li, X. Zhou, Z. Bian, Y. Xing, J. Song, Thermal tuning of the interfacial adhesive layer on the band gaps in a one-dimensional phononic crystal, Compos. Struct. 172 (2017) 311–318.
[52] Z.G. Huang, T.T. Wu, Temperature effect on the bandgaps of surface and bulk acoustic waves in two-dimensional phononic crystals, IEEE Trans. Ultrason. Ferr. 52 (2005) 365–370.
[53] M.I. Hussein, M.J. Leamy, M. Ruzzene, Dynamics of phononic materials and structures: historical origins, recent progress, and future outlook, Appl. Mech. Rev. 66 (2014) 040802.
[54] C. He, X. Ni, H. Ge, X.C. Sun, Y.B. Chen, M.H. Lu, X.P. Liu, Y.F. Chen, Acoustic topological insulator and robust one-way sound transport, Nat. Phys. 12 (2016) 1124–1130.
[55] Z.W. Zhang, Q. Wei, Y. Cheng, T. Zhang, D.J. Wu, X.J. Liu, Topological creation of acoustic pseudospin multipoles in a flow-free symmetry-broken metamaterial lattice, Phys. Rev. Lett. 118 (2017) 084303.
[56] L.H. Wu, X. Hu, Scheme for achieving a topological photonic crystal by using dielectric material, Phys. Rev. Lett. 114 (2015) 223901.